Macromolecules

Article

pubs.acs.org/Macromolecules

Self-Assembly and Photoinduced Optical Anisotropy in Dendronized Supramolecular Azopolymers

Jesús del Barrio,*[,†] Eva Blasco,[‡] Chris Toprakcioglu,[§] Alexandros Koutsioubas,[∥] Oren A. Scherman,[†] Luis Oriol,*[,‡] and Carlos Sánchez-Somolinos*[,⊥]

[†]Melville Laboratory for Polymer Synthesis, Department of Chemistry, University of Cambridge, Cambridge CB2 1EW, United Kingdom

[‡]Departamento de Química Orgánica, Facultad de Ciencias-Instituto de Ciencia de Materiales de Aragón, Universidad de Zaragoza-CSIC, 50009 Zaragoza, Spain

[§]Department of Physics, University of Patras, Patras 26500, Greece

[∥]Jülich Centre for Neutron Science, Forschungszentrum Jülich GmbH, Außenstelle am FRM-II, c/o TU München, Lichtenbergstraße 1, 85747 Garching, Germany

[⊥]Departamento de Física de la Materia Condensada, Facultad de Ciencias, Instituto de Ciencia de Materiales de Aragón (ICMA), Universidad de Zaragoza-CSIC, 50009 Zaragoza, Spain

Supporting Information

ABSTRACT: Herein we report the preparation and characterization of dendronized supramolecular polymers composed of a carboxy-terminated azodendron, dAZO, and two different vinylpyridine-containing polymers: poly(4-vinylpyridine) (P4VP) and polystyrene-*b*-poly(4-vinylpyridine) (PS-*b*-P4VP) block copolymer. P4VP can selectively complex dAZO through hydrogen-bonding interactions, thus resulting in liquid crystalline materials. Additionally, this strategy is also applicable to the preparation of dendronized supramolecular block copolymers (BCs). Lamellar, cylindrical, and spherical morphologies are observed for the BC complexes depending on the dAZO to vinylpyridine repeating unit ratio. Photoinduced orientation of the azobenzene moieties is obtained in films of the H-bonded materials—both P4VP and PS-*b*-P4VP based complexes—by using 488 nm linearly polarized light and characterized through birefringence and dichroism measurements. High and stable values of birefringence are obtained for polymers with azobenzene content as low as 2.7 wt %, thus demonstrating the benefits of preorganization in photoactive dendritic moieties in side-chain H-bonded materials.

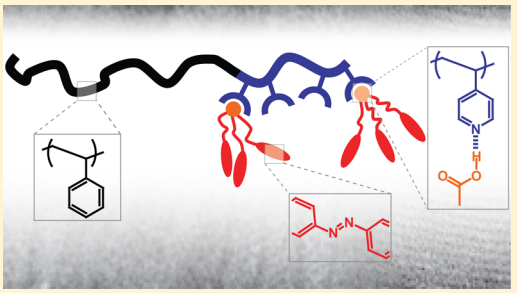

1. INTRODUCTION

The photochromic properties of azobenzene derivatives have been widely investigated for many different applications in recent decades, and their use has enormously grown from colorants, through to optical materials, and most recently in a variety of biologically relevant systems.[1−5] In the field of optical applications specifically, much effort has been focused on the development of azobenzene-containing polymeric materials showing high and stable values of photoinduced anisotropy after irradiation with polarized light (normally in the blue-green region of visible light).[6,7] Some particular applications such as volume holography require thick films (hundreds of micrometers in thickness) with sufficient light penetration, thus photosensitive materials with good optical photoresponse, low levels of scattering, and low optical absorption at the recording wavelength are required.[8,9] In the past few years several groups including our own have investigated azobenzene-containing block copolymers (BCs) for this purpose.[10−13] These copolymers are generally composed of two different blocks—one containing the azobenzene units and a second block which does not absorb at the recording wavelength. High and stable values of photoinduced anisotropy have been found for some of these systems with low chromophore content. However, the synthesis of well-defined functional BCs is, in general, a demanding, expensive and time-consuming process. In contrast, a two-component mixture consisting of a small molecule azobenzene moiety and a BC-based scaffold is a plausable, facile, and inexpensive approach to prepare photochromic BCs.

In this regard, the groups of Ikkala and ten Brinke have pioneered research on supramolecular comb coil hydrogen-bonded polymers based on H-acceptor polymers, including commercially available poly(styrene-*b*-4-vinylpyridine) (PS-*b*-P4VP), and a variety of H-donor surfactant-type molecules.[14−16] The concept of attaching small molecules to vinylpyridine group-containing polymers has been exploited by Priimagi and co-workers on poly(4-vinylpyridine) (P4VP)

Received: November 15, 2013
Revised: January 8, 2014

   dx.doi.org/10.1021/ma402369p | *Macromolecules* XXXX, XXX, XXX−XXX

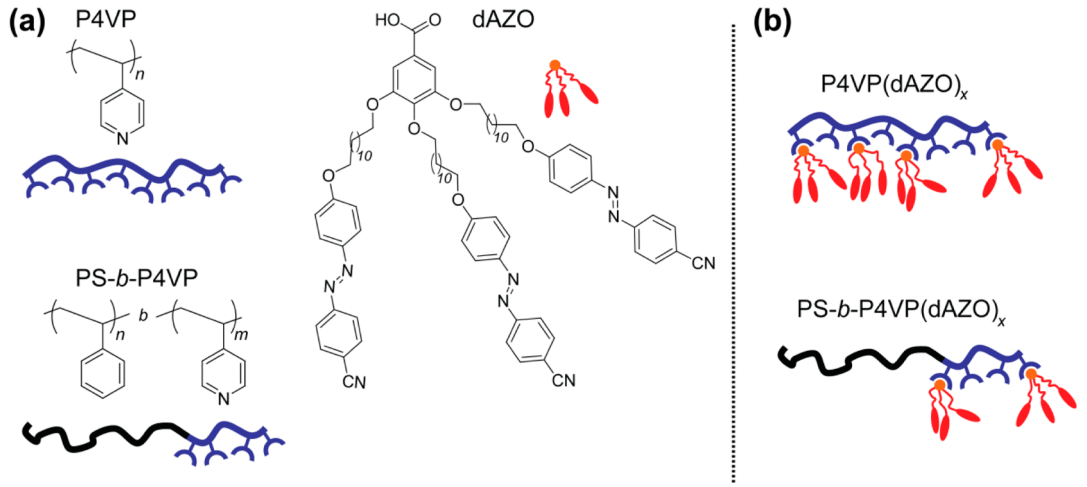

Figure 1. Chemical structures and schematic representations of (a) P4VP and PS-*b*-P4VP polymers and dAZO azodendron together with (b) the schematic representations of P4VP(dAZO)$_x$ and PS-*b*-P4VP(dAZO)$_x$.

complexed with a variety of azobenzene compounds.[17−20] The same group has investigated the photoinduction of optical anisotropy and the inscription of surface relief grating in thin films of hydrogen-bonded P4VP homopolymers.[17,19,20] A similar strategy can be expanded to BC systems to attain good control of the microsegregated morphology through azobenzene doping.[21] We have recently investigated a series of H-bonded materials comprised of 6-[4-(4′-cyanophenylazo)-phenyloxy]hexanoic acid and PS-*b*-P4VP, which show well-segregated morphologies and good photoresponse at higher degrees of chromophore loading.[22] These materials, however, are limited as their optical response drastically worsens at low chromophore content.

Herein we document the hydrogen-bonding-assisted self-assembly of dAZO, an H-donor azodendron, and two H-acceptor polymers containing vinylpyridine repeating units: P4VP and PS-*b*-P4VP BCs (Figure 1). Azodendron dAZO consists of three promesogenic and photochromic azobenzene moieties and a single carboxylic acid group at the focal point. The dendritic structure of dAZO favors the interaction between pendant azobenzene units, thus enhancing the photoresponse of the complexes in comparison to previously described hydrogen-bonded azopolymers.[22] The series of homopolymer-type complexes P4VP(dAZO)$_x$ consists of dAZO and P4VP (Figure 1). We have also investigated the BC-type series of complexes PS-*b*-P4VP(dAZO)$_x$ composed of dAZO and a particular PS-*b*-P4VP (Figure 1). For both series of complexes, we have systematically altered their degree of complexation *x*, i.e., azodendron to vinylpyridine repeating unit ratio (Table 1), in order to investigate its effect on the thermal, mesomorphic, morphological, and photoinduced optical properties of the self-assembled materials. The P4VP block of PS-*b*-P4VP(dAZO)$_x$ can selectively encapsulate the dAZO moieties whereas the PS block confers processability and transparency to the system—both attractive qualities in optical applications. Photoinduced orientation of the azobenzene units was obtained in films of the supramolecular complexes by using 488 nm linearly polarized light. The achieved photoinduced anisotropy was characterized through birefringence and dichroism measurements.

2. EXPERIMENTAL SECTION

Materials. P4VP homopolymer (M_n = 19 kDa, M_w/M_n = 1.15) and PS-*b*-P4VP diblock copolymer ($M_{n,PS}$ = 24 kDa, $M_{n,P4VP}$ = 1.9 kDa, M_w/M_n = 1.10) were purchased from Polymer Source, Inc., and used without further purification. The preparation of azodendron dAZO was carried out according to the synthetic pathway shown in Scheme 1. 4-Cyano-4′-hydroxyazobenzene was synthesized according to previously described methods.[23] The rest of the starting materials were purchased from Sigma-Aldrich and used without further purification.

Table 1. Composition of the Supramolecular Complexes

complex	*x*	P4VP(dAZO) (wt %)	dAZO (wt %)	chromophore[a] (wt %)
P4VP(dAZO)$_x$	0.06		44.3	22.1
	0.12		61.4	30.6
	0.25		76.1	37.9
	0.50		86.4	43.0
PS-*b*-P4VP(dAZO)$_x$				
	0.06	12.4	5.5	2.7
	0.12	17.0	10.5	5.2
	0.25	24.9	18.9	9.4
	0.50	36.8	31.8	15.9

[a]Weight percentage of chromophoric azo units (4-oxy-4′-cyanoazobenzene).

*4-Cyano-4′-(12″-bromododecyloxy)azobenzene (**1**).* A mixture of 4-cyano-4′-hydroxyazobenzene (2.40 g, 10.8 mmol), 1,12-dibromododecane (17.6 g, 53.8 mmol), finely ground potassium carbonate (3.00 g, 21.7 mmol), potassium iodide (0.25 g, 1.5 mmol), and butan-2-one (50 mL) was stirred and heated to reflux for 16 h. The mixture was then allowed to cool down to room temperature (RT), and the solids were filtered off and washed with acetone. The combined organic solvents were evaporated under reduced pressure to dryness. The residue was purified by flash chromatography using hexane/ethyl acetate (4:1) to yield the required product as an orange solid. Yield: 3.50 g (69%). ^{1}H NMR (400 MHz, $CDCl_3$, δ): 7.97−7.90 (m, 4H), 7.79 (d, J = 8.3 Hz, 2H), 7.02 (d, J = 8.8 Hz, 2H), 4.06 (t, J = 6.5 Hz, 2H), 3.41 (t, J = 6.8 Hz, 2H), 1.90−1.77 (m, 4H), 1.53−1.23 (m, 16H). ^{13}C NMR (100 MHz, $CDCl_3$, δ): 162.74, 154.79, 146.67, 133.14, 125.45, 123.05, 118.66, 114.86, 113.10, 68.47, 34.05, 32.81, 29.50−29.33, 29.12, 28.74, 28.15, 25.97. IR (KBr, cm^{-1}): 2227, 1600, 1468, 1256, 1140, 860, 842.

*Methyl 3,4,5-Tris[12-(4-(4′-cyanophenyldiazo)phenoxy)-dodecyloxy)]benzoate (**2**).* A mixture of 4-cyano-4′-(12″-bromododecyloxy)azobenzene (2.00 g, 4.25 mmol), methyl gallate (0.23 g, 1.2 mmol), finely ground potassium carbonate (0.90 g, 6.5 mmol), potassium iodide (0.11 g, 0.66 mmol), and butan-2-one (30 mL) was stirred and heated to reflux for 24 h. The mixture was allowed

dx.doi.org/10.1021/ma402369p | Macromolecules XXXX, XXX, XXX−XXX

Scheme 1. Synthesis of Azodendron dAZO

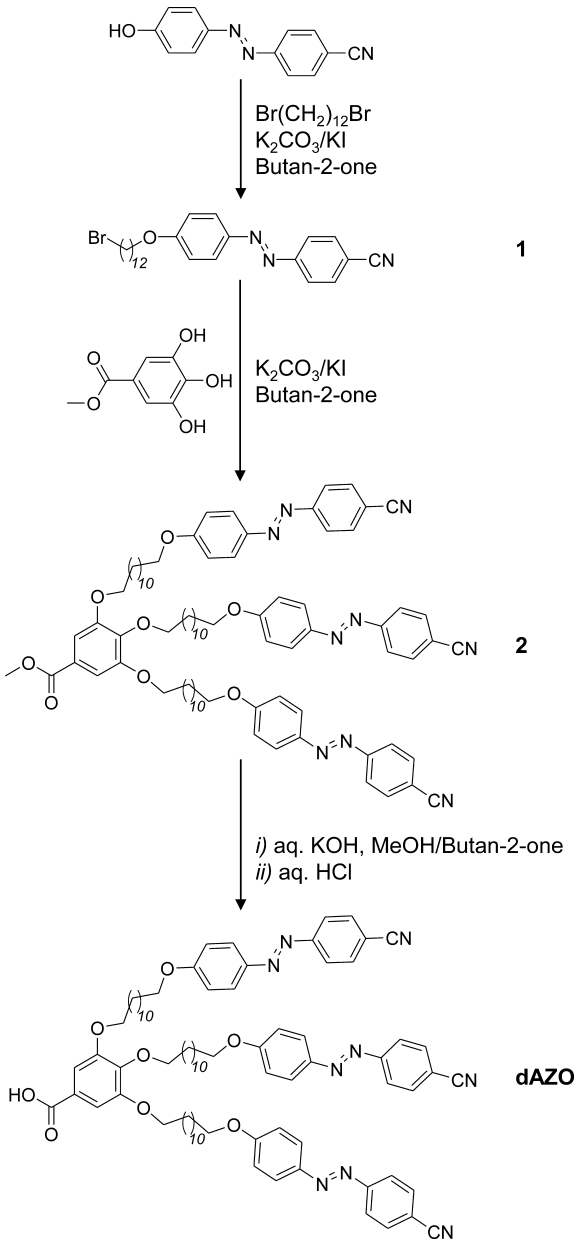

to cool down to RT, and the solids were filtered off and washed with acetone. The combined organic solvents were evaporated under reduced pressure to dryness. The residue was purified by flash chromatography on silica gel and eluted with dichloromethane, gradually changing the composition of the eluent to 1:20, ethyl acetate:dichloromethane. Yield: 3.10 g (54%). ^{1}H NMR (400 MHz, $CDCl_3$, δ): 7.99−7.89 (m, 12H), 7.80−7.75 (m, 6H), 7.27 (s, 2H), 7.05−6.98 (m, 6H), 4.09−3.97 (m, 12H), 3.89 (s, 3H), 1.88−1.70 (m, 12H), 1.54−1.25 (m, 48H). ^{13}C NMR (100 MHz, $CDCl_3$, δ): 166.89, 162.72, 154.80, 152.78, 146.66, 133.13, 125.44, 124.69, 123.04, 118.69, 118.58, 114.84, 113.15, 108.01, 73.39, 69.12, 68.46, 52.14, 30.36−29.06, 26.04−25.96. IR (KBr, cm^{-1}): 2228, 1717, 1601, 1472, 1252, 1139, 849. MALDI-TOF MS Calcd for $C_{83}H_{101}N_9NaO_8$ $[M + Na]^+$: 1374.8; found: 1375.9.

3,4,5-Tris[12-(4-(4′-cyanophenyldiazo)phenoxy)dodecyloxy)]-benzoic Acid (dAZO). A mixture of compound **2** (2.00 g, 1.48 mmol), methanol (25 mL), and aqueous potassium hydroxide (10 mL, 4M) was heated under reflux, and the evolution of the reaction was followed by thin layer chromatography. When all the starting material had been consumed, the reaction mixture was neutralized with concentrated hydrochloric acid. Then, the organic solvents were evaporated under reduced pressure, and the crude product was filtered off and washed with water. The product was purified by flash chromatography on silica gel and eluted with dichloromethane, gradually increasing the polarity of the eluent with methanol. Yield: 0.85 g (43%). ^{1}H NMR (400 MHz, $CDCl_3$, δ): 7.95−7.89 (m, 12H), 7.80−7.75 (m, 6H), 7.31 (s, 2H), 7.03−6.96 (m, 6H), 4.07−3.97 (m, 12H), 1.87−1.69 (m, 12H), 1.53−1.24 (m, 48H). ^{13}C NMR (100 MHz, $CDCl_3$, δ): 170. 85, 162.70, 154.71, 152.84, 146.63, 133.12, 128.40, 125.18, 123.03, 122.66, 118.60, 114.77, 113.07, 108.42, 73.47, 69.12, 68.41, 30.28, 29.91−28.99, 26.14−25.73. IR (KBr, cm^{-1}): 3240, 3070, 2640, 2580, 2226, 1682, 1250, 1139, 842. MALDI-TOF MS calcd for $C_{82}H_{100}N_9O_8$ $[M + H]^+$: 1338.8; found: 1338.8; calcd for $C_{82}H_{99}N_9NaO_8$ $[M + Na]^+$: 1360.8; found: 1360.8. Anal. Calcd for $C_{82}H_{99}N_9O_8$: C, 73.57; H, 7.45; N, 9.42; found: C, 73.46; H, 7.46; N, 9.18.

Sample Preparation. Supramolecular complexes P4VP(dAZO)$_x$ and PS-*b*-P4VP(dAZO)$_x$ consist of mixtures of dAZO and the polymers P4VP and PS-*b*-P4VP, respectively. In the complex names, x denotes the number of dAZO moieties per vinylpyridine repeating unit. The compositions of all the complexes are listed in Table 1. P4VP(dAZO)$_x$ complexes were prepared as follows. The required amounts of P4VP and dAZO were first weighted and dissolved separately in chloroform to form 1−2% (w/v) stock solutions. Then, the P4VP solution was added dropwise to the dAZO solution followed by stirring overnight at RT. Finally, the solvent was slowly evaporated, and the mixtures were dried under vacuum at 40 °C for 2 days. PS-*b*-P4VP(dAZO)$_x$ complexes were prepared in an analogous manner from tetrahydrofuran solutions of dAZO and the BC.

Characterization Techniques. IR spectra were obtained on a Nicolet Avatar 360-FT-IR spectrophotometer using KBr pellets. Thermogravimetric analysis was performed using a TA Q5000IR instrument at a heating rate of 10 °C min^{-1} under a nitrogen atmosphere. Mesogenic behavior was evaluated by POM using an Olympus BH-2 polarizing microscope fitted with a Linkam THMS600 hot stage. Thermal transitions were determined by DSC using a TA DSC Q-2000 instrument under a nitrogen atmosphere with powdered samples (about 3 mg) sealed in aluminum pans. Glass transition temperatures were determined at the midpoint of the baseline jump. Other phase transition temperatures different from T_g were read at the maximum of the corresponding peaks. XRD measurements were performed with an evacuated Pinhole camera (Anton−Paar) operating with a point-focused Ni-filtered Cu K beam. The patterns were collected on flat photographic films perpendicular to the X-ray beam. Powdered samples of the supramolecular complexes were placed into quartz Lindemann capillaries (1 mm diameter). SAXS experiments were performed at the SWING beamline of the French synchrotron facility SOLEIL. The X-ray wavelength of λ = 1.24 Å and sample−detector distance of D = 2000 mm corresponded to a scattering wavevector range of 0.005 Å^{-1} < Q < 0.5 Å^{-1}. The beam path was held under vacuum conditions, except for a path length of about 1 cm, around the sample. Then scattering data (40 frames of 1 s duration for each sample) were collected with a 17 × 17 cm^2 low-noise AVIEX CCD detector. The 2D scattering images were radially averaged, divided by the transmitted intensity, and finally averaged for each sample.

Transmission Electron Microscopy Observations. P4VP-(dAZO)$_x$ samples for TEM analyses were prepared as follows. The complexes were dissolved in chloroform to obtain solutions with a concentration of 1 mg/mL. Thin films of the complexes were then prepared by drop-casting the polymer solutions onto carbon-coated copper grids (previously treated in a UV-ozone chamber for 1 min) followed by thermal annealing. In order to enhance the contrast, the films were exposed to ruthenium oxide (RuO_4) vapor for 1 h before the measurement. The staining agent was purchased from Poly-Sciences and used without further purification. In the case of PS-*b*-P4VP(dAZO)$_x$, the samples were prepared as follows. A few milligrams of each material was heated at 200 °C for 1 min and simultaneously molded to form a pellet with a rectangular prism shape. After this process, the sample was rapidly quenched to RT. Ultrathin

dx.doi.org/10.1021/ma402369p | *Macromolecules* XXXX, XXX, XXX−XXX

sections of about 50 nm were obtained from the thermally annealed samples using a Leica ultramicrotome (model EM UC6) equipped with a diamond knife (Diatome ultra 35°) and picked up on carbon-coated copper grids. The sections were then exposed to RuO_4 vapor for 1 h at RT to enhance contrast. The staining agent RuO_4 was purchased from PolySciences and used without further purification. A JEOL-2000 FXIII microscope operating at 200 kV was employed for all the observations.

Optical Measurements in Films. Thin films of P4VP(dAZO)$_x$ for optical measurements were prepared by casting from chloroform solutions of the supramolecular complexes onto clean glass substrates. In the case of PS-*b*-P4VP(dAZO)$_x$ tetrahydrofuran (good solvent of the material) was used instead of chloroform. The films were heated up to 200 °C for 1 min and rapidly quenched to RT (by putting the films onto a cold aluminum plate) before performing the optical measurements. The thickness of the thermally treated films was measured using a DEKTAK profilometer, with values in the range of 0.1−4.0 μm. A Varian Cary 500 UV−vis−IR spectrophotometer was used for optical absorption and dichroism measurements. For the latter measurements a linear polarizer was introduced in front of the film. The dichroic ratio is defined as the ratio of the maximum absorption measured using linearly polarized light perpendicular and parallel to the polarization of the 488 nm beam, respectively. Birefringence (Δn) measurements were performed using a standard setup reported elsewhere.[12] The sample was placed between crossed polarizers with their polarization directions at ±45° with the vertical axis and irradiated with vertically polarized 488 nm light from an Ar^+ laser. The light from a 633 nm He−Ne laser (30 mW) transmitted through the polarizer−sample−polarizer system was measured with a Si photodetector. It was confirmed that 633 nm light at this power did not introduce any significant change in the optical properties of the film. The transmitted intensity I is given by eq 1:

$$I = I_0 \sin^2(\pi|\Delta n|d/\lambda) \quad (1)$$

where I_0 is the intensity transmitted by the "as quenched" films between parallel polarizers, d the film thickness, and λ the wavelength of the measuring light (633 nm).

3. RESULTS AND DISCUSSION

3.1. Preparation and Characterization of dAZO Azodendron and P4VP(dAZO)$_x$ Supramolecular Complexes. Azodendron dAZO was obtained following the convergent synthetic approach depicted in Scheme 1. In the first step, 4-cyano-4′-hydroxyazobenzene is alkylated with and excess of 1,12-dibromododecane under standard Williamson etherifications conditions to yield **1**. Subsequent etherification with methyl gallate under similar conditions yielded **2**. Target dAZO was obtained by alkaline hydrolysis of the methyl ester group of **2**. The evolution of the saponification reaction was monitored by FT-IR spectroscopy—the shift of the carbonyl stretching absorbance toward longer wavelengths (from 1717 to 1682 cm^{-1}), together with the appearance of the band associated with the O−H stretching of the aromatic carboxylic acid group of dAZO at 3420 cm^{-1}, indicated the successful hydrolysis of the methyl ester group of **2**. The azodendron was purified using standard column chromatography techniques and fully characterized. The ^{1}H NMR spectrum of the azodendron is consistent with the proposed chemical structure and confirmed the purity of this compound (Figure S1). In addition, mass spectrometric analysis of dAZO showed the expected peak, and no other signals corresponding to dendrons with a partial functionalization or traces of nonhydrolyzed ester **2** were detected. With dAZO in hand, the supramolecular complexes P4VP(dAZO)$_x$ were prepared by mixing chloroform solutions of the corresponding amount of polymer and azodendron followed by slow evaporation at RT. In order to investigate the influence of dAZO weight fraction on the thermal and photoinduced optical properties of the complexes, the degree of complexation was varied systematically between x = 0.50 and x = 0.06. Complexes with these x's are fully miscible supramolecular blends with also relatively high loading of azobenzene chromophore (Table 1). For homogenization purposes, all the mixtures were heated for 1 min at 200 °C, a temperature well above both the melting point of dAZO and the glass transition (T_g) of P4VP (see the thermal characterization section), and then rapidly quenched to RT. The samples obtained in this way appeared as homogeneous materials, and this provided the first evidence for the complete miscibility of the individual components (*vide infra*). The formation of hydrogen-bonding interactions was first investigated by FT-IR. The FT-IR spectrum of dAZO together with those of P4VP(AZO)$_{0.50}$ and P4VP are shown in Figure 2. In the case

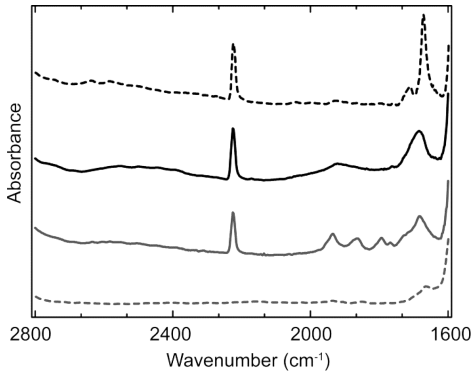

Figure 2. IR spectra of azodendron dAZO (black dashed line), P4VP(dAZO)$_{0.50}$ (black full line), PS-*b*-P4VP(dAZO)$_{0.50}$ (gray full line), and P4VP (gray dashed line).

of the azodendron, the stretching modes and Fermi resonances of the hydroxyl groups involved in hydrogen-bonded dimers are detected as three bands at 3070, 2640, and 2580 cm^{-1}. The appearance of two new bands around 2500 cm^{-1} (broad band) and 1940 cm^{-1} in the spectra of the complexes are attributed to the O−H stretching band and its Fermi resonance of nonionic OH groups bound to pyridine groups. Also, nonassociated pyridine groups of P4VP contribute to the absorption at 992 cm^{-1}. However, the intensity of this band decreases in P4VP(AZO)$_x$, and a new absorption peak is detected at 1014 cm^{-1}, which is related to pyridine rings involved in hydrogen bonding.[24] Additionally, the carbonyl band of dAZO shifts from 1682 to 1700 cm^{-1}, indicating the formation of hydrogen-bonding interactions between the carboxylic acid group of dAZO and the pyridine groups of P4VP.[25]

3.2. Thermal Characterization of P4VP(dAZO)$_x$ Supramolecular Complexes. The thermal stability of the P4VP homopolymer and azodendron dAZO was studied by thermogravimetry (TGA) using powdered samples. The polymer and the azodendron showed good thermal stability up to 250 °C, with onsets of decomposition at temperatures higher than 300 °C (Figure S2). The thermal and thermodynamic properties of the supramolecular complexes P4VP(dAZO)$_x$ together with those corresponding to their individual components, P4VP and dAZO, were studied by polarizing optical microscopy (POM) and differential scanning calorimetry (DSC). While P4VP is an amorphous polymer (T_g ∼ 140 °C), dAZO exhibits monotropic liquid crystalline behavior, with a melting transition at 151 °C and an isotropic-

dx.doi.org/10.1021/ma402369p | Macromolecules XXXX, XXX, XXX−XXX

to-mesophase transition at 140 °C (detected on the DSC by using a sweep rate of 10 °C/min; see Figure S3). The liquid crystalline phase was classified as SmA on account of the fan-shaped textures observed by POM (Figure S4). A latent heat value at the I−SmA transition of $\Delta H_{I-SmA} \sim 13$ kJ mol^{-1} was obtained. The combination of dAZO and P4VP leads to supramolecular complexes with different thermal properties than those exhibited by the individual components. It has been previously shown that the noncovalent grafting of low molecular weight pro-mesogenic or mesogenic compounds to a non-mesomorphic polymer chain can lead to liquid crystalline polymeric materials.[26] Mesomorphic textures were indeed observed by POM for P4VP(dAZO)$_x$, which showed enantiotropic mesomorphism (contrarily to the monotropic behavior of dAZO). The DSC traces for P4VP(dAZO)$_x$ collected on heating at 10 °C/min are shown in Figure 3,

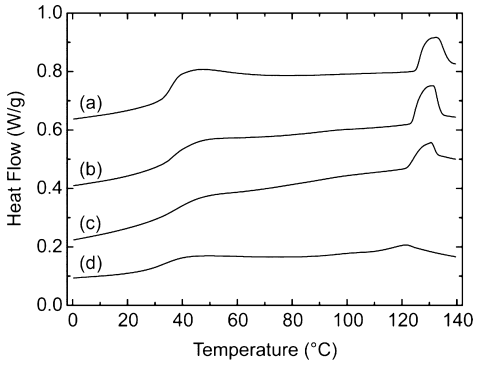

Figure 3. DSC thermograms of (a) P4VP(dAZO)$_{0.50}$, (b) P4VP(dAZO)$_{0.25}$, (c) P4VP(dAZO)$_{0.12}$, and (d) P4VP(dAZO)$_{0.06}$ corresponding to the second heating cycle at a sweep rate of 10 °C/min (endotherms are shown upward).

and the corresponding thermal transitions are gathered in Table 2. A single T_g was detected at 34−37 °C on the heating process which is considerably reduced when compared to the T_g of pure P4VP. A similar feature has already been described for other noncovalent azobenzene-containing polymers and attributed to a plasticization effect of dAZO hydrogen-bonded

Table 2. Transition Temperatures of dAZO and P4VP(dAZO)$_x$ Supramolecular Complexes

supramolecular complex		T_g[a] (°C)	T_i[a] (°C) [ΔH_i (kJ mol^{-1})]	ΔH_i/au[b] (kJ mol^{-1})
dAZO	2nd cool		140 [13]	4.3
P4VP(dAZO)$_{0.50}$	2nd heat	36	132 [790]	2.9
	2nd cool	26	130 [1080]	4.0
P4VP(dAZO)$_{0.25}$	2nd heat	37	130 [410]	3.0
	2nd cool	23	128 [560]	4.1
P4VP(dAZO)$_{0.12}$	2nd heat	37	131 [200]	2.9
	2nd cool	22	127 [288]	4.2
P4VP(dAZO)$_{0.06}$	2nd heat	34	121 [95]	2.8
	2nd cool	21	115 [138]	4.1

[a]Transition temperatures were determined by DSC from the second heating/cooling scan (10 °C min^{-1}). T_g is the glass transition temperature determined at the midpoint of the heat capacity increase. T_i is the mesophase-to-isotropic transition temperature read at the maximum of the peak, and ΔH_i is the corresponding enthalpy. [b]ΔH_i/au is the enthalpy of the mesophase-to-isotropic transition per azobenzene unit.

to the polymer.[17] Additionally to the T_g, an endothermic peak is also detected on heating at around 120−130 °C.[27] This transition was identified as the mesophase-to-isotropic transition due to the disappearance of the liquid crystal textures observed under the POM. Mesomorphic textures were detected again when P4VP(dAZO)$_x$ samples were cooled down from the isotropic state. The nature of the liquid crystalline phase could, however, not be unambiguously determined by POM observations due to the poorly defined textures (Figure S5). The enthalpy change per azobenzene unit at the isotropic-to-mesophase transition (ΔH_i/au in Table 2) for P4VP(dAZO)$_x$ is ca. 4 kJ mol^{-1}, a value which is comparable to that of neat dAZO. Therefore, the interaction strength between the azobenzene units is similar for these complexes regardless of x, and it is not affected after blending dAZO with a non-mesomorphic material such as P4VP. This is also supported by the fact that the complexes show similar mesophase temperature range.

In order to gain further insight into the organization of the liquid crystalline phases of P4VP(dAZO)$_x$, transmission electron microscopy (TEM) observations were performed on stained samples of the complexes. The samples were prepared by casting solutions of the complexes onto copper grids followed by thermal annealing (the samples were heated to 200 °C for 1 min and then rapidly quenched to RT) and subsequent staining with RuO_4. A clear layered structure with a periodicity of ca. 40 Å is observed, and this could be indicative of smectic-type liquid crystalline behavior (a TEM image of the complex with $x = 0.50$ is shown in Figure S6 as a representative example).[28] The smectic nature of the mesophase was further evidenced by XRD studies. The results for a P4VP(dAZO)$_{0.25}$ fiber sample drawn from the isotropic phase are discussed here as a representative example. Specimens of the complex were obtained by heating a powdered sample at 200 °C for 1 min immediately followed by drawing from the melt (thus resulting in a fast quenching of the drawn fiber). The diffractogram of these fibers consists of a pair of arcs perpendicular to the fiber axis (drawing direction) that corresponds to a layer spacing of ca. 39 Å (Figure S7). The orientation of the arcs indicates that the smectic layers orient parallel to the flow direction upon drawing. In addition, a diffuse halo is also detected in the 4−5 Å range, which is typically associated with the distance between mesogenic units. The molecular length of dAZO and a pyridine repeating unit estimated with Dreiding stereomodels for their fully extended conformations are 36 and 5 Å, respectively. Since the calculated length of a dendron bound to a pyridine repeating unit is comparable to the experimentally obtained smectic spacing, a monolayer structure is a reasonable model for the SmA mesophase of the complexes. No significant differences of the smectic spacing were detected for the rest of the complexes by XRD analysis.

3.3. Preparation and Characterization of PS-*b*-P4VP(dAZO)$_x$ Supramolecular Complexes. The confinement of azobenzene chromophores in one of the blocks of azo-BCs allows achieving further reduction of the chromophore fraction compared to homopolymer systems while preserving favorable interactions between photoactive moieties within the azo domains.[6] Therefore, we combined dAZO with a PS-*b*-P4VP BC composed of a PS block (nonabsorbing polymer at the recording wavelength) and a P4VP block which can be complexed with H-donor moieties. The general structure of these complexes is schematically represented in Figure 1, and their compositions are gathered in Table 1. We have prepared

dx.doi.org/10.1021/ma402369p | Macromolecules XXXX, XXX, XXX−XXX

complexes with similar degrees of complexation to those of P4VP(dAZO)$_x$, for the sake of comparison. PS-*b*-P4VP-(dAZO)$_x$ was prepared by dissolving the neat BC in tetrahydrofuran (1−2% w/v solution) and then adding the desired amount of dAZO dissolved in the same solvent. Afterward, the solvent was allowed to evaporate at RT, and the complexes were dried in a vacuum oven at 40 °C. The samples were heated to 200 °C for 1 min and then rapidly quenched to RT in order to erase any thermal history of the material. FT-IR studies verified the formation of hydrogen-bonding interactions between the pyridine groups and dAZO [a partial FT-IR spectra of PS-*b*-P4VP(dAZO)$_{0.50}$ is shown in Figure 2, as an example]. The appearance of new bands around 2500 and 1940 cm^{-1} in the spectra of the complexes was attributed to nonionic O−H···N bonds, similarly to the homopolymer-based complexes. Also, the characteristic peaks of self-associated carboxylic groups at 2640 and 2580 cm^{-1} are not detected in the complex, thus confirming the absence of dAZO dimers.

3.4. Thermal Characterization and Morphological study of PS-*b*-P4VP(dAZO)$_x$ Supramolecular Complexes.

Two distinct levels of hierarchical self-assembly can take place in PS-*b*-P4VP(dAZO)$_x$ complexes: (a) the liquid crystalline organization within the P4VP(dAZO) domains and (b) the phase-separated structure due to segregation between PS and P4VP(dAZO) blocks.[15] The hierarchical self-assembly of the complexes together with their thermodynamic and liquid crystalline properties were characterized by a combination of techniques including DSC, POM, XRD, and TEM. The neat BC is an amorphous material, and as the P4VP weight fraction is relatively small, only the T_g corresponding to the PS block ($T_g \sim 95$ °C) was detected. As it can be anticipated from previous results, the efficient incorporation of dAZO into the P4VP segment significantly modifies the thermal properties of the individual building blocks, both the BC and the H-donor dendron. Similarly to P4VP complexes, mesomorphic properties were detected for PS-*b*-P4VP(dAZO)$_x$ (Table 1). Thermally treated samples of the complexes were studied by POM and XRD in order to determine their liquid crystalline phases. Textures observed under the polarized-light optical microscope were poorly defined, as expected for complexes with low dAZO weight fraction (Figures S8 and S9). A progressive fading and eventual disappearance of the textures was observed between 175 and 195 °C. We have previously shown that P4VP(dAZO)$_x$ self-assembles into a smectic-type liquid crystalline organization. The same type of arrangement is also present in PS-*b*-P4VP(dAZO)$_x$ which was verified by XRD studies. All PS-*b*-P4VP(dAZO)$_x$ complexes show a diffuse halo in the wide angle region corresponding to a distance of 4.5 Å, which is associated with the average distance between mesogenic moieties (Figure S10a shows, as a representative example, an X-ray diffraction pattern of a powder sample of PS-*b*-P4VP(dAZO)$_{0.25}$ heated at 200 °C for 1 min followed by quenching to RT). Also, the absence of sharp Bragg reflections in the WAXS profiles of the samples confirms that the formation of crystallized species is fully avoided, at least on the time scale of the measurements. The scattering peaks related to the smectic liquid crystalline domains of PS-*b*-P4VP(dAZO)$_x$, q and the second order $2q$, are present in the SAXS intensity profiles for all x's and correspond to a layer spacing of 4.4 nm (peaks at $q > 0.1$ Å^{-1} in Figure 4), which is similar to the smectic spacing of P4VP(dAZO)$_x$.

The main thermal transitions of PS-*b*-P4VP(dAZO)$_x$ were also investigated by DSC. The DSC curves of PS-*b*-P4VP-(dAZO)$_x$ collected on heating at 10 °C/min are depicted in Figure 5, and the transitions are gathered in Table 3. Two clear

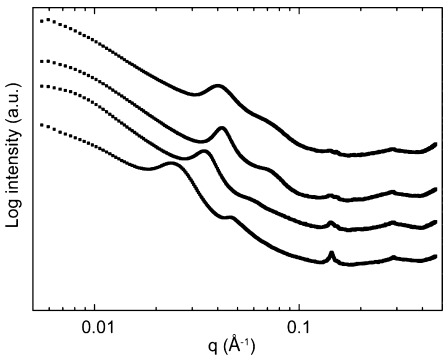

Figure 4. SAXS intensity profiles of samples of PS-*b*-P4VP(dAZO)$_{0.50}$, PS-*b*-P4VP(dAZO)$_{0.25}$, PS-*b*-P4VP(dAZO)$_{0.12}$, and PS-*b*-P4VP-(dAZO)$_{0.06}$ (from bottom to top) heated at 200 °C and fast quenched to RT.

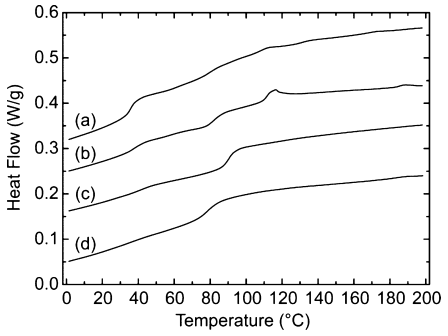

Figure 5. DSC thermograms of (a) PS-*b*-P4VP(dAZO)$_{0.50}$, (b) PS-*b*-P4VP(dAZO)$_{0.25}$, (c) PS-*b*-P4VP(dAZO)$_{0.12}$, and (d) PS-*b*-P4VP-(dAZO)$_{0.06}$ corresponding to the second heating cycle at a sweep rate of 10 °C/min (endotherms are shown upward).

Table 3. Transition Temperatures of PS-*b*-P4VP(dAZO)$_x$ Supramolecular Complexes

supramolecular complex		T_{g1}[a] (°C)	T_{g2}[a] (°C)	T_i[a] (°C)	T_{ODT} (°C)
PS-*b*-P4VP(dAZO)$_{0.50}$					
	2nd heat	36	80	112	173
	2nd cool	24	67	126	
PS-*b*-P4VP(dAZO)$_{0.25}$					
	2nd heat	38	82	117	189
	2nd cool	27	69		178
PS-*b*-P4VP(dAZO)$_{0.12}$					
	2nd heat	38	90		
	2nd cool	40	80		
PS-*b*-P4VP(dAZO)$_{0.06}$					
	2nd heat	28	76		189
	2nd cool	22	68		176

[a]Transition temperatures were determined by DSC from the second heating scan (10 °C min^{-1}). T_g is the glass transition temperature determined at the midpoint of the heat capacity increase. T_i is the mesophase-to-isotropic transition temperature read at the maximum of the peak.

dx.doi.org/10.1021/ma402369p | *Macromolecules* XXXX, XXX, XXX−XXX

T_gs were detected for all the complexes. The transition at lower temperature corresponds to the P4VP(dAZO) block while the one at higher temperature is associated with the PS block. The P4VP(dAZO) block T_g range is similar to that of the homopolymer-based series. On the other hand, the PS T_g is slightly reduced when compared to the neat BC, a feature that might be related to the plasticization effect of a minor fraction of nonbound dAZO dispersed in the PS domains. Additionally to the T_gs, two endotermic peaks were identified on the heating scans of each of the two complexes with higher degree of complexation. While no significant changes of the mesomorphic textures were observed at the lower temperature transition, the disappearance of the textures (at 175−195 °C) for all PS-*b*-P4VP(dAZO)$_x$ is related to the transition at higher temperature. We have preliminary assigned the lower temperature transition to the isotropization of the liquid crystalline ordering (T_i in Table 3) of the P4VP(dAZO) domains as it is relatively close to the smectic-to-isotropic transition temperature of P4VP(dAZO)$_x$ complexes. This feature was confirmed by the disappearance of the smectic halo in the XRD patterns of PS-*b*-P4VP(dAZO)$_{0.50}$ and PS-*b*-P4VP(dAZO)$_{0.25}$ at temperatures higher than T_i (Figure S10). Since the isotropization of the smectic ordering is likely to take place at around 110−120 °C but the birefringent textures persist at higher temperatures, we have tentatively assigned the second endothermic peak to the order-to-disorder phase transition of the supramolecular BCs (order-to-disorder transition, T_{ODT} in Table 3).

The phase segregation of diblock copolymers, A-*b*-B, is typically dictated by the Flory−Huggins interaction parameter, χ, the degree of polymerization, N, and the volume fraction of the blocks, f_A and f_B. In general, diblock copolymers with a low value for χN show a disordered state disregarding the volume fraction of the blocks. For volume fractions of the minority block and χN values above certain limits, diblock copolymers can show different microphase-separated states depending on the volume fraction of the blocks. Matsen and Bates have predicted the phase diagram of diclock copolymers in between the weak ($\chi N \leq 10$) and the strong segregation regime ($\chi N \geq 10$) where spherical, cylindrical, and lamellar morphologies are described for increasing volume fractions of the minor block.[29,30] Assuming that PS and P4VP(AZO) are the two distinct blocks and also that the phase behavior of PS-*b*-P4VP(dAZO)$_x$ will be analogous to a regular diblock copolymer, the selective incorporation of dAZO into the P4VP domains of the parent BC can alter its original morphology on account of a change in its composition (i.e., volume fraction of the blocks) as well as the interaction parameter. Also, the induction of liquid crystalline properties may affect the phase separation behavior.[31,32] We have studied the microdomain morphology of the parent diblock copolymer as well as those of the supramolecular BC complexes by TEM. As described in the Experimental Section, the samples were heated at 200 °C for 1 min and rapidly quenched to RT. Ultrathin sections were stained with RuO_4 and studied by TEM. No clear phase separation was observed for the parent PS-*b*-P4VP (Figure S11). Typical TEM bright-field images corresponding to the supramolecular complexes are shown in Figure 6. A clear lamellar morphology was found for PS-*b*-P4VP(dAZO)$_{0.50}$. In the cases of PS-*b*-P4VP(dAZO)$_{0.25}$, PS-*b*-P4VP(dAZO)$_{0.12}$, and P4VP(dAZO)$_{0.06}$, the segregated morphologies could be consistent with both cylindrical and spherical morphologies. SAXS measurements performed on thermally treated samples (annealing at 200 °C for 1 min and subsequent quenching to RT) allowed us to clarify which are the types of segregated morphologies of the complexes as well as the domain spacings. The SAXS intensity profiles of PS-*b*-P4VP(dAZO)$_x$ are shown in Figure 4. The scattering peaks in the $q < 0.1$ Å^{-1} region of PS-*b*-P4VP(dAZO)$_{0.50}$ are at a ratio of 1:2, which is characteristic for a lamellar morphology. The domain spacing is calculated to be about 26 nm. Two scattering signals are also observed in the $q < 0.1$ Å^{-1} region of the scattering profiles of PS-*b*-P4VP(dAZO)$_{0.25}$ and PS-*b*-P4VP(dAZO)$_{0.12}$—one intense peak at lower q and another one at higher q, which appears as a shoulder of the main peak. These two signals are at a ratio of 1:$\sqrt{3}$ and indicate a hexagonally packed cylinder structure with domain spacing between the (100) planes of 18 and 15 nm for $x = 0.25$ and $x = 0.12$, respectively. The reflections in the SAXS profile of PS-*b*-P4VP(dAZO)$_{0.06}$ are not as well resolved as in the cases above; however, in comparison to PS-*b*-P4VP(dAZO)$_{0.25}$ and PS-*b*-P4VP(dAZO)$_{0.12}$, the main peak at lower q is shifted toward lower q values, which may indicate a body-centered cubic sphere structure. In general, these results are in agreement with the previously presented diagram for BCs. The different morphologies of the complexes are related to the changes in their composition. The parent BC did not show clear phase separation. However, an increase in the weight fraction of the P4VP block after complexation—from a P4VP weight fraction of 0.07 of the parent PS-*b*-P4VP to a P4VP(dAZO) weight fraction of 0.12 for PS-*b*-P4VP(dAZO)$_{0.06}$—induces the formation of segregated microstructures, probably with a body-centered cubic sphere structure. Several groups including our own have observed spherical morphologies for H-bonded complexes based on sphere-forming PS-*b*-P4VP with similar weight fraction to PS-*b*-P4VP(dAZO)$_{0.06}$.[22,33] As x increases, the evolution of morphologies, from spherical ($x = 0.06$), to cylindrical ($x = 0.12, 0.25$), and eventually to lamellar phases ($x = 0.50$), is ascribed to the increase in the weight fraction of the P4VP(dAZO) block and qualitatively follows the typical phase diagram predicted for BCs. Also, the presence of anisotropic liquid crystalline phases probably favors the stabilization of lamellar and cylindrical morphologies at relatively low P4VP(dAZO)$_x$ weight fractions. It has been suggested that the addition of H-donor additives to PS-*b*-P4VP might decrease the χ parameter between PS and P4VP (thus changing the value for χN accordingly);[34] however, it may still remain in the strong segregation regime as microphase-separated structures have been observed even at low x.

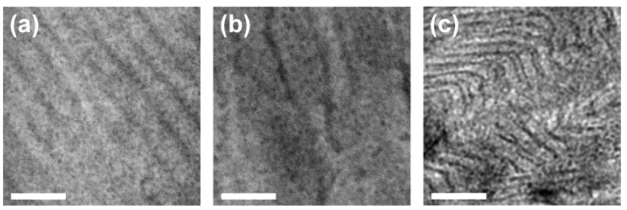

Figure 6. TEM bright-field micrographs of (a) PS-*b*-P4VP(dAZO)$_{0.06}$, (b) PS-*b*-P4VP(dAZO)$_{0.25}$, and (c) PS-*b*-P4VP(dAZO)$_{0.50}$ (the white bar is 100 nm).

3.5. Photoinduced Optical Response. This section includes a discussion on the optical properties of the supramolecular complexes both in solution and in the solid state and also a study on the photoinduced optical anisotropy in films of the title compounds. The spectrum corresponding to dAZO dissolved in chloroform is characterized by a strong and

dx.doi.org/10.1021/ma402369p | Macromolecules XXXX, XXX, XXX−XXX

quite symmetric band with a maximum at 367 nm, corresponding to the $\pi-\pi^*$ transition of the *trans*-cyanoazobenzene moiety, and a weak band in the 450 nm region associated with the $n-\pi^*$ transition of the same configurational isomer (Figure S12). No significant changes were found in the absorption spectra of the supramolecular complexes in solution (Figure 7). Films for optical measurements were obtained by

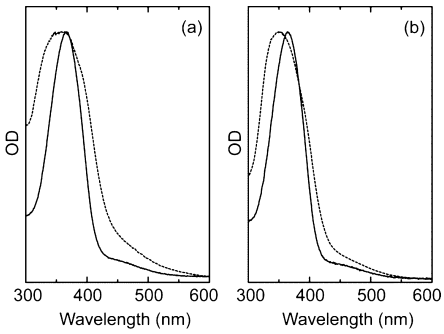

Figure 7. UV−vis absorption spectra of P4VP(dAZO)$_{0.50}$ (a) and PS-*b*-P4VP(dAZO)$_{0.50}$ (b) in thin film (dashed lines) and in chloroform and tetrahydrofuran solutions, respectively (full lines).

casting solutions of the complexes onto clean glass substrates [chloroform and tetrahydrofuran were used as solvents for P4VP(dAZO)$_x$ and PS-*b*-P4VP(dAZO)$_x$ respectively]. The films were heated at 200 °C for 1 min in order to erase any previous thermal history and then rapidly cooled down to RT. The main absorption band is clearly broadened and shifted toward shorter wavelengths in the absorption spectra of the films (Figure 7). These features are more pronounced in the complexes with higher x and have been previously attributed to chromophore−chromophore intermolecular interactions.[19,35]

Photoinduced anisotropy has been extensively reported in a broad variety of azobenzene-containing materials.[36−39] This phenomenon is due to the preferential orientation of azobenzene chromophores with their long axis perpendicular to the light polarization direction through *trans*−*cis*−*trans* photoinduced isomerization cycles.[1] In our case, optical anisotropy was induced in thermally treated films of the complexes by using 488 nm linearly polarized light (2.8 W/cm^2). After a 60 min irradiation period, the samples were kept in darkness and the birefringence was monitored for further 30 min. As representative examples, Figure 8 shows the evolution of $|\Delta n|$ for the complexes with $x = 0.25$. Birefringence increased by the action of polarized light until saturation. When the 488 nm light was switched off, $|\Delta n|$ either remained constant or slightly increased until quickly reaching a final stable value (the increase in birefringence after switching off the light was always smaller than 5−10% of the $|\Delta n|$ saturation value at the end of the irradiation period). A similar qualitative evolution of the $|\Delta n|$ was found for the rest of the complexes. Also, the same values of $|\Delta n|$ were obtained for samples of the same material with different thickness (film thickness values in the range of 0.1−4.0 μm). As $|\Delta n|$ depends on the azobenzene content, we discuss our results in terms of normalized photoinduced birefringence $|\Delta n|_{norm}$ which is obtained by dividing $|\Delta n|$ by the azobenzene content of the supramolecular complex (AZO wt % in Table 1). The final $|\Delta n|_{norm}$ values after the irradiation and relaxation periods for all the complexes are gathered in Table 4. Final $|\Delta n|_{norm}$ values were approximately constant for each of the series of complexes with $|\Delta n|_{norm}$ = 0.0015−0.0016 for

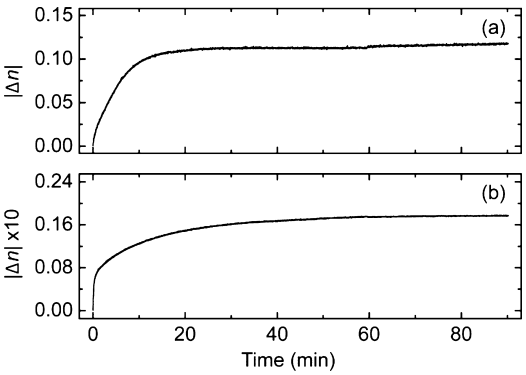

Figure 8. Evolution of the photoinduced birefringence in thermally treated films of complexes (a) P4VP(dAZO)$_{0.25}$ and (b) PS-*b*-P4VP(dAZO)$_{0.25}$ under irradiation with 488 nm linearly polarized (films were irradiated between t = 0 and t = 60 min).

Table 4. Values of $|\Delta n|_{norm}$[a] after the Irradiation and Relaxation Periods and Equilibrium Dichroic Ratio

complex	x	$\|\Delta n\|_{norm} \times 10^3$	dichroic ratio
P4VP(dAZO)$_x$	0.06	1.5	4.9
	0.12	1.6	4.9
	0.25	1.6	5.3
	0.50	1.6	5.5
PS-*b*-P4VP(dAZO)$_x$	0.06	0.87	3.2
	0.12	0.97	4.0
	0.25	0.94	3.8
	0.50	0.94	3.7

[a] $|\Delta n|_{norm}$ is obtained by dividing $|\Delta n|$ by the azobenzene content of the supramolecular complex (AZO wt % in Table 1).

P4VP(dAZO)$_x$ and $|\Delta n|_{norm} \sim 0.0009$ for PS-*b*-P4VP(dAZO)$_x$. In all cases, the photoinduced birefringence could be completely erased by thermal annealing, i.e., heating at 200 °C for 1 min followed by quenching to RT.

Dichroism measurements were performed on films of the complexes to further characterize the photoinduced optical anisotropy. The polarized optical absorption spectra corresponding to films of P4VP(dAZO)$_{0.25}$ and PS-*b*-P4VP(dAZO)$_{0.25}$ irradiated in the same conditions as in the photoinduced anisotropy experiments are gathered in Figure 9 as representative examples (the polarized optical absorption spectra of all the complexes are shown in Figure S13). The

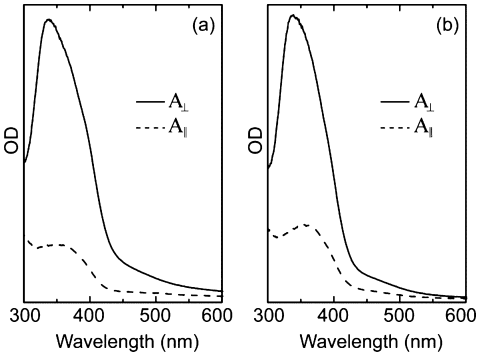

Figure 9. Stable polarized absorption spectra of (a) P4VP(dAZO)$_{0.25}$ and (b) PS-*b*-P4VP(dAZO)$_{0.25}$ measured at RT after irradiation with 488 nm linearly polarized light for 60 min and subsequent evolution in darkness for 30 min at the same temperature.

dx.doi.org/10.1021/ma402369p | *Macromolecules* XXXX, XXX, XXX−XXX

measuring light was polarized either perpendicular or parallel to the polarization direction of the 488 nm light. The equilibrium dichroic ratios obtained after the irradiation and relaxation periods for all the studied complexes are gathered in Table 4. High and stable dichroic ratios were obtained for the complexes with values in the ranges 4.9−5.5 and 3.2−4.0 for P4VP-$(dAZO)_x$ and PS-*b*-P4VP$(dAZO)_x$, respectively. The slightly lower values of $|\Delta n|_{norm}$ and dichroic ratios of PS-*b*-P4VP-$(dAZO)_x$ could be attributed to the inherent phase-separated nature of the BC-derived complexes, which can partially hinder photo-orientation processes. Overall, the photoinduced response of P4VP$(dAZO)_x$ and PS-*b*-P4VP$(dAZO)_x$ is higher and more stable than to that of recently reported systems based on 6-[4-(4′-cyanophenylazo)phenyloxy]hexanoic acid. This clearly highlights the benefits of preorganizing the photochromic moieties in the dendritic tecton dAZO. The final $|\Delta n|_{norm}$ values do not substantially decrease at lower *x*—in contrast to other supramolecular azopolymers[19,20,22]—thus allowing for a larger reduction of the azobenzene content without any detrimental effect on $|\Delta n|_{norm}$. Although it is still unclear why $|\Delta n|_{norm}$ does not depend on *x*, dendritic liquid crystal tectons such as dAZO—with preorganized azobenzene moieties—could induce favorable interdendron cooperative interactions during complexation. Moreover, they are known to enhance mesogen-to-mesogen interactions,[32] thus resulting in higher degrees of photoinduced order.

4. CONCLUSIONS

In summary, we have demonstrated the preparation of photoaddressable dendronized polymers through hydrogen bonding by mixing a carboxy-terminated azodendron and commercially available P4VP and PS-*b*-P4VP polymers. Liquid crystalline materials have been obtained even for low ratios of dAZO to vinylpyridine repeating unit. The BC complexes showed mesomorphic behavior and exhibited two T_gs as well as two higher temperature transitions. Spherical, cylindrical, and lamellar morphologies were observed for the PS-*b*-P4VP complexes depending on *x*. In contrast to our previous system, which showed low degree of photoinduced order at lower *x*,[22] higher ($|\Delta n|_{norm} \sim 0.0009$) and stable photoinduced optical response are obtained for dAZO-containing complexes even at azobenzene contents as low as 2.7 wt %, thus evidencing the benefits of using this dendritic tecton with preorganized photochromic moieties in side-chain supramolecular azopolymers. We have shown that materials with enhanced optical properties can be readily produced through the combination of molecular self-assembly and "chromophore synthons" with optimized design. We expect that the field of responsive materials will greatly benefit from this versatile method as it significantly facilitates gaining fundamental understanding on the optical response of photoaddressable polymers.

■ ASSOCIATED CONTENT

Supporting Information

Thermal characterization of dAZO, polarized optical micrographs of dAZO and the H-bonded complexes, supplementary TEM bright-field micrographs and X-ray diffraction patterns of the parent PS-*b*-P4VP and the H-bonded complexes, and UV−vis absorption spectrum of dAZO in solution. This material is available free of charge via the Internet at http://pubs.acs.org.

■ AUTHOR INFORMATION

Corresponding Authors

*E-mail: jd529@cam.ac.uk (J.d.B.).
*E-mail: loriol@unizar.es (L.O.).
*E-mail: carloss@unizar.es (C.S.S.).

Notes

The authors declare no competing financial interest.

■ ACKNOWLEDGMENTS

The authors acknowledge Dr. Mª Ángeles Laguna of the Servicio de Microscopía Electrónica-Universidad de Zaragoza for her help with TEM image analyses. Eva Blaso acknowledges a JAE-predoc grant. This work was supported by the MICINN, Spain, under the project MAT2011-27978-C02-01 and MAT2011-27978-C02-02, FEDER and DGA funding.

■ REFERENCES

(1) Natanshon, A.; Rochon, P. *Chem. Rev.* **2002**, *102*, 4139−4175.
(2) Yu, H.; Ikeda, Y. *Adv. Mater.* **2011**, *23*, 2149−2180.
(3) Goulet-Hanssens, A.; Barrett, C. J. *J. Polym. Sci., Part A: Polym. Chem.* **2013**, *51*, 3058−3070.
(4) Sebai, S. C.; Milioni, D.; Walrant, A.; Alves, I. D.; Sagan, S.; Huin, C.; Auvray, L.; Massotte, D.; Cribier, S.; Tribet, S. *Angew. Chem., Int. Ed.* **2012**, *51*, 2132−2136.
(5) del Barrio, J.; Horton, P. N.; Lairez, D.; Lloyd, G. O.; Toprakcioglu, C.; Scherman, O. A. *J. Am. Chem. Soc.* **2013**, *135*, 11760−11763.
(6) Hvilsted, S.; Sánchez, S.; Alcalá, R. *J. Mater. Chem.* **2009**, *19*, 6641−6648.
(7) Audorff, H.; Kreger, K.; Walker, R.; Haarer, D.; Kador, L.; Schmidt, H. W. In *Advances in Polymer Science*; Müller, A. H. E., Schmidt, H. W., Eds.; Springer-Verlag: Berlin, 2010; Vol. *228*.
(8) Hagen, R.; Bieringer, T. *Adv. Mater.* **2001**, *13*, 1805−1810.
(9) Matharu, A. S.; Jeeva, S.; Ramanujam, P. S. *Chem. Soc. Rev.* **2007**, *36*, 1868−1880.
(10) Frenz, C.; Fuchs, A.; Schmidt, H. W.; Theissen, U.; Haarer, D. *Macromol. Chem. Phys.* **2004**, *205*, 1246−1258.
(11) Häckel, M.; Kador, L.; Kropp, D.; Frenz, C.; Schmidt, H. W. *Adv. Funct. Mater.* **2005**, *15*, 1722−1727.
(12) Forcén, P.; Oriol, L.; Sánchez, C.; Alcalá, R.; Hvilsted, S.; Jankova, K.; Loos, J. *J. Polym. Sci., Part A: Polym. Chem.* **2007**, *45*, 1899−1910.
(13) Berges, C.; Oriol, L.; Piñol, M.; Sánchez-Somolinos, C.; Alcalá, R. *Opt. Mater.* **2013**, *35*, 1095−1098.
(14) Ikkala, O.; ten Brinke, G. *Science* **2002**, *295*, 2407−2409.
(15) Ikkala, O.; ten Brinke, G. *Chem. Commun.* **2004**, 2131−2137.
(16) ten Brinke, G.; Roukolainen, J.; Ikkala, O. In *Advances in Polymer Science*; Binder, W., Ed.; Springer-Verlag: Berlin, 2007; Vol. *207*.
(17) Vapaavuori, J.; Priimagi, A.; Kaivola, M. *J. Mater. Chem.* **2010**, *20*, 5260−5264.
(18) Priimagi, A.; Saccone, M.; Cavallo, G.; Shishido, A.; Pilati, T.; Metrangolo, P.; Resnati, G. *Adv. Mater.* **2012**, *24*, OP345−OP352.
(19) Priimagi, A.; Vapaavuori, J.; Rodríguez, F. J.; Faul, C. F. J.; Heino, M. T.; Ikkala, O.; Kauranen, M.; Kaivola, M. *Chem. Mater.* **2008**, *20*, 6358−6363.
(20) Koskela, J. E.; Vapaavuori, J.; Hautala, J.; Priimagi, A.; Faul, C. F. J.; Kaivola, M.; Ras, R. H. A. *J. Phys. Chem. C* **2012**, *116*, 2362−2370.
(21) Kuila, B. K.; Stamm, M. *J. Mater. Chem.* **2011**, *21*, 14127−14134.
(22) del Barrio, J.; Blasco, E.; Oriol, L.; Alcalá, R.; Sánchez-Somolinos, C. *J. Polym. Sci., Part A: Polym. Chem.* **2013**, *51*, 1716−1725.
(23) del Barrio, J.; Oriol, L.; Alcalá, R.; Sánchez, C. *J. Polym. Sci., Part A: Polym. Chem.* **2010**, *48*, 1538−1550.
(24) Lee, J. Y.; Painter, P. C.; Coleman, M. M. *Macromolecules* **1988**, *21*, 954−960.

(25) Chuang, W. T.; Sheu, H. S.; Jeng, U. S.; Wu, H. H.; Hong, P. D.; Lee, J. J. *Chem. Mater.* **2009**, *21*, 975−978.
(26) Kato, T.; Mizoshita, N.; Kishimoto, K. *Angew. Chem., Int. Ed.* **2006**, *45*, 38−68.
(27) In the case of P4VP(dAZO)$_{0.50}$ an extra endothermic peak was detected at 144 °C in the first DSC heating cycle. This peak cannot be detected on cooling and is almost disappeared in succeeding cycles—its associated ΔH measured in the second heating scan represents less than 4% of ΔH_i of the same cycle. We have preliminary associated this peak to the melting transition of a fraction of dAZO nonbound to P4VP. After the initial heating cycle, however, this fraction is almost negligible, and P4VP(dAZO)$_{0.50}$ can be considered as a fully miscible mixture of dAZO and P4VP.
(28) Korhonen, J. T.; Verho, T.; Rannou, P.; Ikkala, O. *Macromolecules* **2010**, *43*, 1507−1514.
(29) Bates, F. S. *Science* **1991**, *251*, 898−905.
(30) Khandpur, A. K.; Förster, S.; Bates, F. S.; Hamley, I. W.; Ryan, A. J.; Bras, W.; Almdal, K.; Mortensen, K. *Macromolecules* **1995**, *28*, 8796−8806.
(31) Walther, M.; Finkelmann, H. *Prog. Polym. Sci.* **1996**, *21*, 951−979.
(32) del Barrio, J.; Oriol, L.; Alcalá, R.; Sánchez, C. *Macromolecules* **2009**, *42*, 5752−5760.
(33) Ruokolainen, J.; Saariaho, M.; Ikkala, O.; ten Brinke, G.; Thomas, E. L. *Macromolecules* **1999**, *32*, 1152−1158.
(34) Kuila, B. K.; Gowd, E. B.; Stamm, M. *Macromolecules* **2010**, *43*, 7713−7721.
(35) Kelly, A. M. *J. Chem. Phys.* **2003**, *119*, 3320−3331.
(36) Audorff, H.; Walker, R.; Kador, L.; Schmidt, H. W. *Chem.—Eur. J.* **2011**, *17*, 12722−12728.
(37) Hernández-Ainsa, S.; Alcalá, R.; Barberá, J.; Marcos, M.; Sánchez, C.; Serrano, J. L. *Macromolecules* **2010**, *43*, 2660−2663.
(38) Zakrevskyy, Y.; Stumpe, J.; Faul, C. F. J. *Adv. Mater.* **2006**, *18*, 2133−2136.
(39) Hernández-Ainsa, S.; Alcalá, R.; Barberá, J.; Marcos, M.; Sánchez, C.; Serrano, J. L. *Eur. Polym. J.* **2011**, *47*, 311−318.